



Constructing accommodational space in MnO₂ cathode for Mn²⁺ transport and electrodeposition for aqueous zinc-ion batteries

Qiong Wu¹ · Siqi Li¹ · Yuan Han¹ · Chao Yang¹ · Jiangang Gao¹

Received: 9 June 2022 / Revised: 20 June 2022 / Accepted: 22 June 2022 / Published online: 2 July 2022
© The Author(s), under exclusive licence to Springer-Verlag GmbH Germany, part of Springer Nature 2022

Abstract

MnO₂ is the most desirable cathode material for aqueous zinc ion batteries; however, its electrochemical performance is still limited by the problem of structural collapse that inevitably occurs due to the dissolution-deposition mechanism. Here, the structure-induced problems are mitigated by designing physical accommodation space by dissolving the Nano-ZnO template for the MnO₂ cathode. By having facilitated more open surfaces for the electrode reaction and provided channels for the diffusion of Mn²⁺ and Zn²⁺, the physical accommodational space significantly improves the electrochemical performance of the cathode. As expected, the rate and cycling performance of the pore cathode (540.6 mAh g⁻¹ at 0.2 A g⁻¹, 289.5 mAh g⁻¹ at 1.0 A g⁻¹) is superior to that of the normal δ-MnO₂ cathode (406.2 mAh g⁻¹ at 0.2 A g⁻¹, 243.1 mAh g⁻¹ at 1 A g⁻¹), at the same time, the discharge specific capacity is 230% of that of the Regular electrode after 500 cycles at 1.0 A g⁻¹ current density. This simple method of making improvements on made cathodes yields unexpected results, which alleviated the capacity decay of the normal electrode in the first 100 cycles. This study will elucidate the development of high stability cells by constructing better MnO₂ electrodes by an electrode de-template method for zinc ion batteries.

Keywords Aqueous zinc ion battery · MnO₂ cathode · Dissolution-deposition mechanism · Accommodational space

Introduction

Currently, the growing demand for electric vehicles and portable devices has accelerated the development of the battery industry [1]. Due to the limited resources and safety concerns of the mainstream lithium-ion batteries (LIBs) in the battery industry [2], zinc-ion aqueous batteries (ZIBs) possess extensive research significance to become the successor of LIBs due to their safety and large resource storage capacity [3]. ZIBs are a promising new battery system due to their low cost, high operational safety, and environmental friendliness [4, 5]. Zn anodes with a relatively high capacity of 820 mAh g⁻¹, along with excellent chemical stability in neutral and weakly acidic aqueous electrolytes, are a definite advantage for aqueous

ZIBs based on two-electron redox reactions [6–10]. In addition, Zn²⁺ possesses a small ionic radius that facilitates the dissolved deposition of Zn²⁺ ions [11].

Among the numerous cathode materials, including manganese-based oxides [12–14], vanadium-based oxides [15–18] and Prussian blue analogues [19–21] have been developed as promising candidates for ZIBs. Among these, MnO₂ cathode material is the most promising candidate due to the high working voltage (~1.5–1.6 V) and high specific capacity (300–500 mAh/g) of it, achieving the high energy density of the full battery [22]. So far, the reversible Zn²⁺/H⁺ insertion mechanism in the MnO₂ cathode is widely accepted, and it is inevitable that the MnO₂ cathode material will undergo a serious phase transition from the initial structure designed during the charging and discharging process. As a result, these phase transitions during the cycle may cause structural collapse and capacitance decay of the electrode. Various strategic approaches, such as cationic doping (e.g., Mg²⁺ and V⁵⁺), crystal shape regulation (e.g., nanosheets and nanoparticles), and conductive hybridization (e.g., graphene and polyaniline), have been developed to improve storage performance and mitigate capacity decay [23–26].

✉ Chao Yang
yangchaomaterial@126.com

Jiangang Gao
gaojiangang@ahpu.edu.cn

¹ Anhui Laboratory of Clean Energy Materials and Chemistry for Sustainable Conversion of Natural Resources, School of Chemical and Environmental Engineering, Anhui Polytechnic University, Wuhu 241000, China

Despite these achievements, it is found that there exists a dissolution and redeposition mechanism in the positive electrode of MnO_2 , and the structure stability of MnO_2 suffers from the dissolution and redeposition of it during charge and discharge, which results in the inevitable problem of specific capacity decay [27]. To solve or alleviate these problems, it is necessary to form the overall cathode a porous structure to provide channels for the transfer of the Mn^{2+} and Zn^{2+} , and also a specific surface area that facilitates the redeposition of MnO_2 . $\delta\text{-MnO}_2$ has inherent characteristics such as large interlayer spacing in its layered structure, which is beneficial to the transfer of ions as an active material in batteries. Herein, an accommodational space cathode (named AS cathode) with the structure of accommodation space was constructed by obtaining a simple method of dissolving part of the nano ZnO template.

Experimental

Preparation of MnO_2

A concentrated 1 ml of H_2SO_4 was added drop by drop into the 500 ml 0.02 M KMnO_4 solution which then take 0.015 ml of MnSO_4 dissolved in 500 ml of distilled water and stir well. Under stirring, the dissolved KMnO_4 solution and MnSO_4 solution are poured together into a 1 L beaker to react for 2 h and precipitate for 12 h.

Preparation of AS cathode

The obtained MnO_2 and nano ZnO, conductive carbon (super P) and PVDF, are ground evenly in a ratio of 7:4:2:1, and the material is spread flat on the steel foil with NMP as dispersant and dried at 120 °C for 12 h to obtain the cathode with template (named as Templated cathode). The nano ZnO particles in Templated cathode were removed partially by immersed and washed by 0.01 mol/L HCl for 6 h. The treated cathode was repeatedly washed with pure water and dried for 12 h to have obtained AS cathode. A control MnO_2 cathode the same mass ratio containing MnO_2 and no nano ZnO template was obtained using the same procedure as above (named as Regular cathode).

Material characterization

The synthesized MnO_2 was characterized and analyzed by an X-ray diffractometer (XRD, Rigaku D). A scanning electron microscope (SEM Hitachi S4800) was used to observe the surface and cross-sectional morphology of the cathode before and after de-template to determine the structural morphological changes. The chemical states of the elements in cathode after cycling were characterized by X-ray electron spectrometry (XPS, Thermo ESCALAB).

Electrical properties characterization

The homemade Swagelok cells which were assembled by the obtained cathodes, nylon mesh separator, zinc foil anode and 2 M ZnSO_4 + 0.1 M MnSO_4 electrolyte were used to measure the storage capacity of Zn^{2+} at a temperature of 25 °C for the testing of ZIB cells, respectively. The electrochemical charge/discharge tests were performed at room temperature using a CT 2001A system. The cells were tested with a voltage window of 1.0–1.8 V vs. Zn^{2+} , Zn [28]. An electrochemical workstation (CHI 660E) was used to obtain cyclic voltametric (CV) curves, keeping the test voltage window constant.

Experimental results and discussion

Morphology and structure

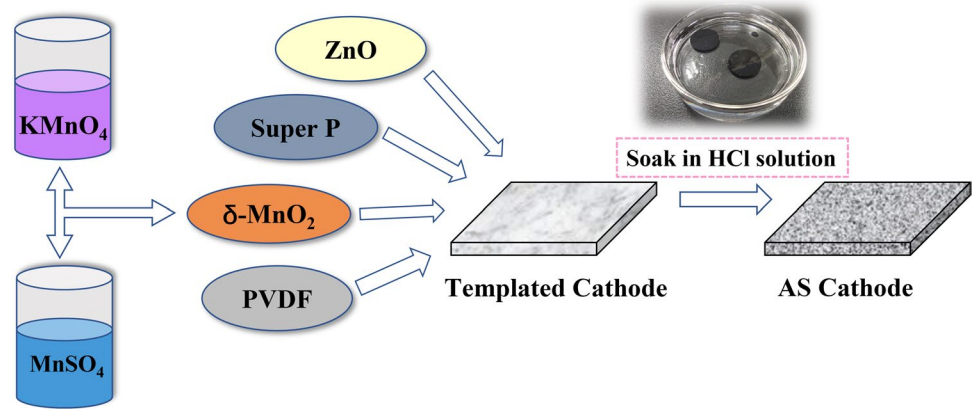
The schematic diagram of the preparation process of MnO_2 and AS cathode is shown in Fig. 1. This method of preparing Nano-to-micron-sized MnO_2 under normal temperature and pressure conditions is very simple and can produce MnO_2 in large quantities. The way to prepare the AS cathode is to directly dissolve the template on the conventional coated cathode sheet, which is an attempt based on the process of industrial production of batteries

Figure 2a shows the composition and lattice morphology of the obtained MnO_2 as observed by XRD. Notably, distinct broad diffraction peaks appear at $2\theta = 12.2^\circ, 24.8^\circ, 37.4^\circ, 42.2^\circ, 66.9^\circ$, which match well with the (003), (006), (101), (015) and (110) facets of JCPDF no.86-0666, indicating the generation of single-phase $\delta\text{-MnO}_2$. Figure 2b, c show the SEM images of the surface of cathode before and after de-template. It can be observed that compared to the Templated cathode, the nano-sized ZnO can no longer be observed and many pore structures clearly appear in the surface of the AS cathode. It should be noted that the de-template does not collapse the original structure, and a solid structure with a high specific surface area of pore cathode material appears. SEM images show an obvious intricate cavity structure in the cross-section of the AS cathode, and at the same time, there are also dense and non-porous flat planes caused by cutting the cathode. The EDS mapping (Fig. 2d, e) reveals that Mn and C are uniformly distributed, which also contain traces of Zn residues (only 0.34% of the total electrode mass).

Electrochemical performance

The CV curves of the AS cathode at a scan rate of 0.1 mV/s for 5 cycles were studied. As shown in Fig. 3a, the same

Fig. 1 The schematic diagram of the preparation process of MnO₂ and AS cathode



anodic peak at 1.56 V was presented in all 5 cycles. The cathode was observed to show two reduction peaks around

1.25 V and 1.38 V during the scans, which are mainly considered as the dissolution of MnO₂ i.e. Mn⁴⁺ (s) → Mn

Fig. 2 **a** XRD curves; **b, c** SEM images before and after de-temple; **d** SEM images of the cross-section and corresponding mapping images of the AS cathode; **e** EDS of the AS cathode

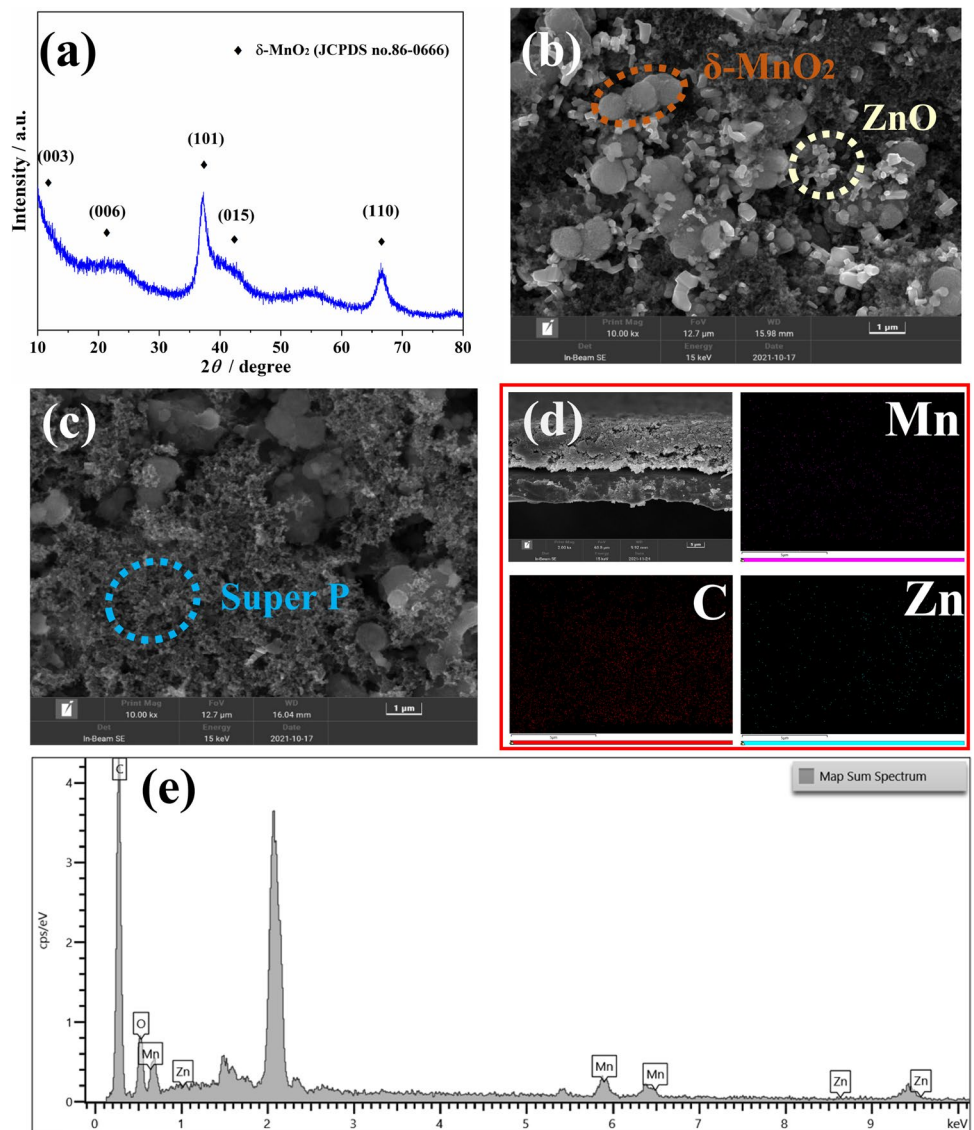
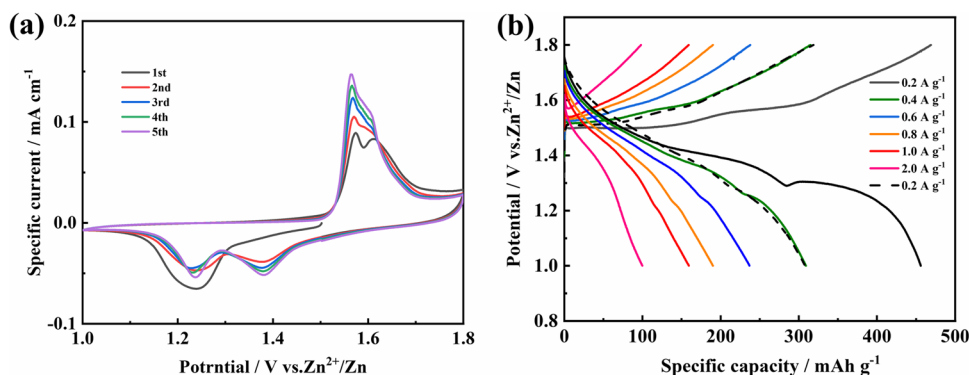


Fig. 3 **a** CV curves; **b** Constant current charge/discharge curves at different current densities of the AS cathode



$^{2+}$ (I) [16]. The CV plot is a stepwise redox process, which is typical of a MnO_2 cathode. Of particular interest is the clear indication of increasing voltametric current as the redox peak was cycled, indicating a gradual electrochemical activation. The specific capacity versus voltage at different current densities is shown in Fig. 3b, which can provide a reversible capacity of 456 mAh g^{-1} at 0.2 A g^{-1} . As the current density increases to 0.4 A g^{-1} , 0.6 A g^{-1} , 0.8 A g^{-1} , 1.0 A g^{-1} , and 2.0 A g^{-1} , the specific capacity is maintained at 309.1 mAh g^{-1} , 236.8 mAh g^{-1} , 190.1 mAh g^{-1} , 159.3 mAh g^{-1} , and 99.7 mAh g^{-1} , respectively, showing excellent rate performance.

Figure 4a shows the discharge-specific capacities of the AS cathode, the Regular cathode, and the Templated cathode at different rates. At a current rate of 0.2 A g^{-1} , the discharge specific capacity of the AS cathode reached 540.6 mAh g^{-1} , which is much higher than that of the Regular cathode (406.2 mAh g^{-1}) and Templated cathode (250 mAh g^{-1}). And, the discharge-specific capacity of the AS cathode was generally higher than that of the other cathodes at different rates. Figure 4b shows the cycling performance of these three cathodes at a high circuit density of 1.0 A g^{-1} . The specific capacities

of Regular cathode and Templated cathode rapid decay from 243.1 mAh g^{-1} to 87.3 mAh g^{-1} and 189.3 mAh g^{-1} to 62.6 mAh g^{-1} in the first 100 cycles respectively; in contrast, the cycle performance of the AS cathode decreases from 289.5 mAh g^{-1} to 190 mAh g^{-1} , which is obviously better than the data for the other two cathodes. This indicates that the accommodation space has a significant effect on improving the discharge-specific capacity and cycle performance of the MnO_2 cathode for ZIBs. It is worth noting that the positive effect of ZnO on water zinc ion battery is excluded by the multiplier and circulation of Template cathode.

The AS cathode after charge/discharge cycles was further investigated by XPS to determine the elemental composition of the cathode material. Figure 5a evaluates the full spectrum, the peaks corresponding to elements of Mn, O, C and Zn can be clearly observed. The Mn 2p spectrum is shown in Fig. 5b, and the two curves in Mn 2p $3/2$ and Mn 2p $1/2$ indicate the presence of trivalent Mn ions and tetravalent Mn ions, respectively. The two peaks appearing in the O 1s spectrum (Fig. 5c) confirm the presence of Mn-O-Mn and H-O-H, respectively [29, 30]. Figure 5d shows the Zn 2p spectrum with two peaks attributed to Zn 2p $3/2$ and Zn 2p

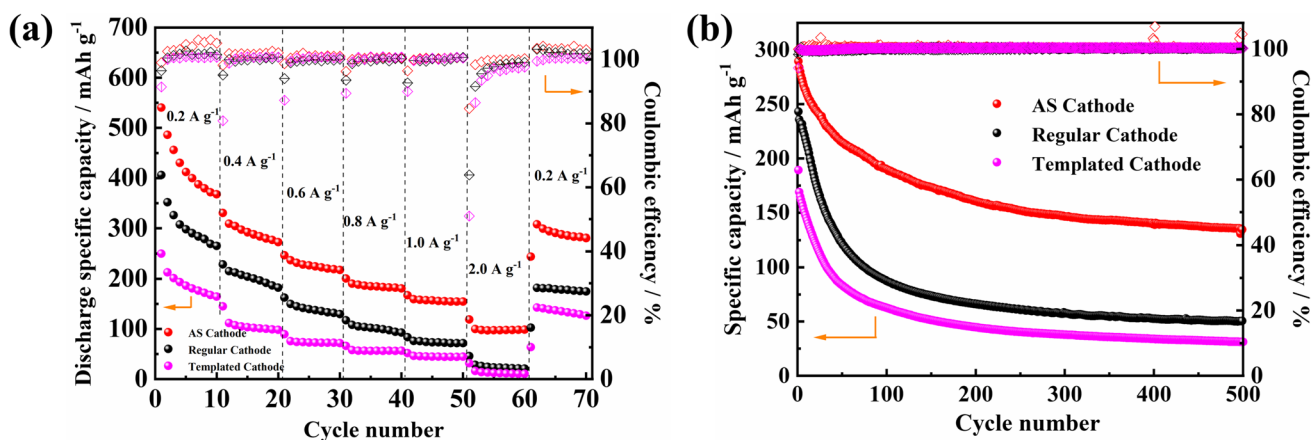
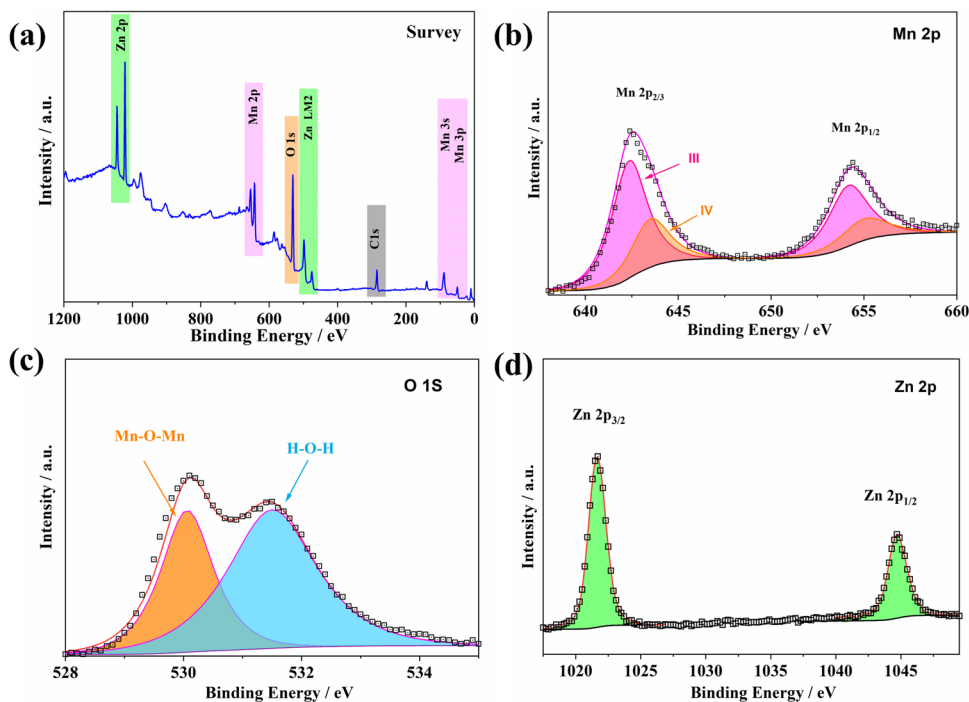


Fig. 4 **a** Rate performance, and **b** long-term cycling stability at 1.0 A g^{-1} of the AS cathode

Fig. 5 **a** XPS spectra of pored cathode, **b** Mn 2p; **c** O 1s and **d** Zn 2p after cycles



1/2 respectively, has shown that the Zn^{2+} enters the cathode material during the charging and discharging process.

Figure 6a shows the CV results at different rates. The current characteristic curve of the redox peak (i , mA) and the scan rate (v , $mV s^{-1}$) at a certain potential conform to the following equation [18, 31].

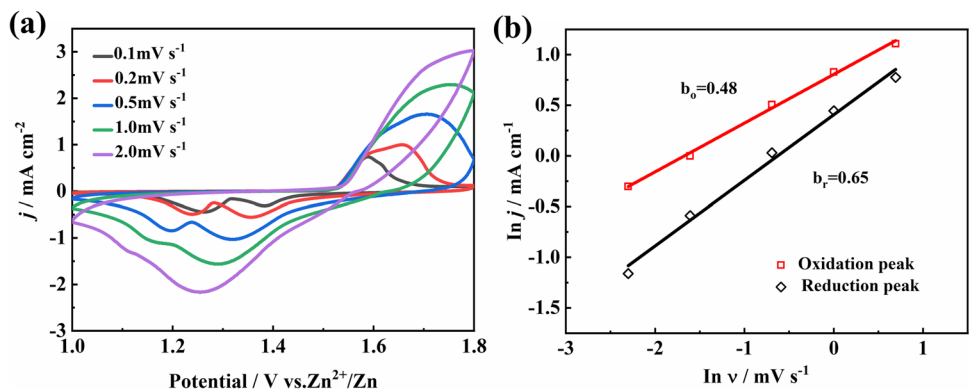
$$i = av^b \tag{1}$$

Furthermore, the relationship $i = av^b$ can be divided into two parts including capacitive (k_1v) and diffusion-limited effects ($k_2v^{1/2}$), as described below

$$i = k_1v + k_2v^{1/2} \tag{2}$$

$$i/v^{1/2} = k_1v^{1/2} + k_2 \tag{3}$$

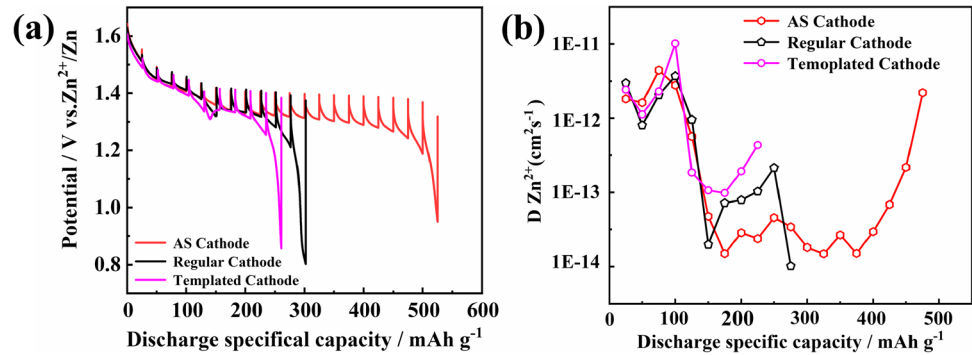
Fig. 6 **a** CV curves at different scan rates, and **b** linear fit of $\log(i)$ versus $\log(v)$ to the redox peaks of the AS cathode



where a and b are empirical values, while $b = 0.5$ indicates the diffusion control electrochemical behavior and $b = 1.0$ indicates surface capacitance process control. Figure 6b shows a linear fit of $\log(i)$ versus $\log(v)$ for the redox peaks. Of note is the high b value of 0.65 for the cathode peak, indicating a joint control of diffusion and surface capacitance process, this is due to the adsorption of SO_4^{2-} on the surface of the cathode while oxidizing Mn^{2+} during the cathodic process. The anode peak has a b -value of 0.48, which indicates diffusion-controlled behavior.

The ion diffusion coefficients of redox reactions were investigated using GITT [32, 33]. Figure 7a, b shows the voltage characteristic curves and the corresponding ion diffusion coefficients of the different battery, respectively. The chemical diffusion coefficient of Zn^{2+} can be calculated based on the following equation:

Fig. 7 **a** GITT curves of different electrodes in discharge state, and **b** corresponding ion diffusion coefficients



$$D_{GITT} = \frac{4}{\pi} \left(\frac{m_B V_m}{m_B S} \right)^2 \left(\frac{\Delta E_s}{\tau (dE_\tau / d\sqrt{\tau})} \right)^2 \quad (4)$$

$$\approx \frac{4}{\pi \tau} \left(\frac{n_m V_m}{S} \right)^2 \left(\frac{\Delta E_s}{\Delta E_\tau} \right)^2 \left(\tau \ll \frac{L^2}{D_{GITT}} \right) \quad (5)$$

where τ is the relaxation time, m_B is the mass of the MnO_2 , M_B , V_m and n_m are shorts for the mass (g), molecular weight (g/mol), molar volume (cm^3/mol) and molal number, respectively. The S is the actual area of the cathode, $\frac{dE_\tau}{d\sqrt{\tau}}$ is the slope of the linearized region of the potential $E\tau$ during the current pulse of duration time τ , ΔE_s is the difference in the open circuit voltage measured at the end of the relaxation period for two successive steps, and L is the thickness of the cathode.

Clearly, it is verified that the reaction kinetics of AS cathode is not better than that of Regular cathode and Templated cathode. This is mainly since the MnO_2 used in the three electrodes is the same. The GITT results prove that the charge-discharge performance of the AS cathode is better than that of the other two cathodes, mainly because the space created after de-template provides an additional place for the deposition of Mn^{2+} . It has been pointed out earlier that, the MnO_2 cathode has a Mn^{2+} dissolution-deposition mechanism during cycling, especially at the back end of charging and discharging. And the Mn^{2+} originally contained in the electrolyte will be oxidized to MnO_2 during charging, which contributes to the improvement of the capacity. The innovation point of our work is that, since Mn^{2+} will eventually be deposited on the surface of the cathode material, the cathode considers the role played by conductive carbon in the charging and discharging process of the battery. On the other hand, the overall design of porous structure for the cathode material increases the specific surface area of the cathode material, which increases the utilization rate of Mn^{2+} while improving the channel for the dissolution redeposition process of it. Thus, the effect of

increasing the specific capacity of battery discharge and mitigating the decay of cycle performance is achieved.

Conclusion

In summary, AS electrodes were successfully prepared by template method, which have been successfully prepared for use as an excellent strategy in MnO_2 cathode ZIBs. AS electrodes which were constructed for ionic dissolution deposition channel have high discharge capacity and good rate capacity at 0.2 A g^{-1} . More importantly, the cell demonstrated excellent cycle durability after 500 cycles, outperforming conventional and template electrodes in hybrid electrolyte of $2.0 \text{ M ZnSO}_4 + 0.1 \text{ M MnSO}_4$. It is believed that the current work will provide a new design strategy for ZIBs cathodes for commercial production of high capacity and long life ZIBs.

Funding This work was supported by the Natural Science Foundation of Anhui Province (NO. 2008085QB78), Anhui Provincial Key Laboratory Open Project Foundation, China (LFCCMCA-05), and The University Synergy Innovation Program of Anhui Province (NO. GXXT-2021-021).

References

- Dunn B, Kamath H, Tarascon J (2011) Electrical energy storage for the grid: a battery of choices. *Science* 334:928–935
- Wen J, Yu Y, Chen C (2012) A review on lithium-ion batteries safety issues: existing problems and possible solutions. *Mater Express* 2:197–212
- Xu C, Li B, Du H, Kang F (2012) Energetic zinc ion chemistry: the rechargeable zinc ion battery. *Angew Chem Int Ed* 51:933–935
- Kuang M, Zhang Y, Li T, Li K, Zhang S, Li G, Zhang W (2015) Tunable synthesis of hierarchical NiCo_2O_4 nanosheets-decorated Cu/CuO_x nanowires architectures for asymmetric electrochemical capacitors. *J Power Sources* 283:270–278
- Baxter J, Bian Z, Chen G, Danielson D, Dresselhaus M, Fedorov A, Fisher T, Jones C, Maginn E, Kortshagen U (2009) Nanoscale design to enable the revolution in renewable energy. *Energy Environ Sci* 2:559–588

6. Huang J, Guo Z, Ma Y, Bin D, Wang Y, Xia Y (2018) Recent progress of rechargeable batteries using mild aqueous electrolytes. *Small Meth* 3:1800272
7. Wang J, Wang J, Liu H, You Z, Wei C, Kang F (2019) Electrochemical activation of commercial MnO microsized particles for high-performance aqueous zinc-ion batteries. *J Power Sources* 438:226951
8. Hao J, Mou J, Zhang J, Dong L, Liu W, Xu C, Kang F (2018) Electrochemically induced spinel-layered phase transition of Mn_3O_4 in high performance neutral aqueous rechargeable zinc battery. *Electrochim Acta* 259:170–178
9. Konarov A, Voronina N, Jo J, Bakenov Z, Sun Y, Myung S (2018) Present and future perspective on electrode materials for rechargeable zinc-ion batteries. *ACS Energy Lett* 3:2620–2640
10. Ming J, Guo J, Xia C, Wang W, Alshareef H (2019) Zinc-ion batteries: materials, mechanisms, and applications. *Mater Sci Eng R* 135:58–84
11. Song H, Lin X, Zhang Y, Wang H, Li H, Huang J (2014) A nanocomposite of needle-like MnO_2 nanowires arrays sandwiched between graphene nanosheets for supercapacitors. *Ceram Int* 40:1251–1255
12. Fang G, Zhou J, Pan A, Liang S (2018) Recent advances in aqueous zinc-ion batteries. *ACS Energy Lett* 3:2480–2501
13. Wang X, Zheng S, Zhou F, Qin J, Shi X, Wang S, Sun C, Bao X, Wu Z (2020) Scalable fabrication of printed Zn// MnO_2 planar micro-batteries with high volumetric energy density and exceptional safety. *Natl Sci Rev* 7:64–72
14. Han M, Huang J, Liang S, Shan L, Xie X, Yi Z, Wang Y, Guo S, Zhou J (2019) Oxygen defects in β - MnO_2 enabling high-performance rechargeable aqueous zinc/manganese dioxide battery. *iScience* 23:100797
15. Yang G, Li Q, Ma K, Hong C, Wang C (2020) The degradation mechanism of vanadium oxide-based aqueous zinc-ion batteries. *J Mater Chem A* 8:8084–8095
16. Zhang N, Dong Y, Jia M, Bian X, Wang Y, Qiu M, Xu J, Liu Y, Jiao L, Cheng F (2018) Rechargeable aqueous Zn- V_2O_5 battery with high energy density and long cycle life. *ACS Energy Lett* 3:1366–1372
17. He P, Yan M, Zhang G, Sun R, Chen L, An Q, Mai L (2017) Layered VS_2 nanosheet-based aqueous Zn ion battery cathode. *Adv Energy Mater* 7:1601920
18. Liu X, Zhang H, Geiger D, Han J, Varzi A, Kaiser U, Moretti A, Passerini S (2019) Calcium vanadate sub-microfibers as highly reversible host cathode material for aqueous zinc-ion batteries. *Chem Commun* 55:2265–2268
19. Paoletta A, Faure C, Timoshevskii V, Marras S, Bertoni G, Guerfi A, Vijn A, Armand M, Zaghbi K (2017) A review on hexacyanoferrate-based materials for energy storage and smart windows: challenges and perspectives. *J Mater Chem A* 5:18919–18932
20. Liu Z, Pulletikurthi G, Endres F (2016) A Prussian blue/zinc secondary battery with a bio-ionic liquid-water mixture as electrolyte. *ACS Appl Mater Interfaces* 8:12158–12164
21. Liu Y, Li Q, Ma K, Yang G, Wang C (2019) Graphene oxide wrapped CuV_2O_6 nanobelts as high-capacity and long-life cathode materials of aqueous zinc-ion batteries. *ACS Nano* 13:12081–12089
22. Zhang N, Cheng F, Liu J, Wang L, Long X, Liu X, Li F, Chen J (2017) Rechargeable aqueous zinc-manganese dioxide batteries with high energy and power densities. *Nat Commun* 8:405
23. Lee J, Ju J, Cho W, Cho B, Oh S (2013) Todorokite-type MnO_2 as a zinc-ion intercalating material. *Electrochim Acta* 112:138–143
24. Alfaruqi M, Islam S, Mathew V, Song J, Kim S, Tung D, Jo J, Kim S, Baboo J, Xiu Z, Kim J (2017) Ambient redox synthesis of vanadium-doped manganese dioxide nanoparticles and their enhanced zinc storage properties. *Appl Surf Sci* 404:435–442
25. Wu B, Zhang G, Yan M, Xiong T, He P, He L, Xu X, Mai L (2018) Graphene scroll-coated α - MnO_2 nanowires as high-performance cathode materials for aqueous Zn-Ion battery. *Small* 14:1703850
26. Huang J, Wang Z, Hou M, Dong X, Liu Y, Wang Y, Xia Y (2018) Polyaniline-intercalated manganese dioxide nanolayers as a high-performance cathode material for an aqueous zinc-ion battery. *Nat Commun* 9:2906
27. Wu T, Lin Y, Althouse Z, Liu N (2021) Dissolution–re-deposition mechanism of the MnO_2 cathode in aqueous zinc-ion batteries. *ACS Appl Energy Mater* 4:12267–12274
28. Pan H, Shao Y, Yan P, Cheng Y, Han K, Nie Z, Wang C, Yang J, Li X, Bhattacharya P, Mueller K, Liu J (2016) Reversible aqueous zinc/manganese oxide energy storage from conversion reactions. *Nat Energy* 1:16039
29. Liu P, Zhu Y, Gao X, Huang Y, Wang Y, Qin S, Zhang Y (2018) Rational construction of bowl-like MnO_2 nanosheets with excellent electrochemical performance for supercapacitor electrodes. *Chem Eng J* 350:79
30. Zhou Q, Zhang L, Zuo P, Wang Y, Yu Z (2018) Enhanced photocatalytic performance of spherical BiOI/ MnO_2 composite and mechanism investigation. *RSC Adv* 8:36161
31. Xia C, Guo J LY, Liang H, Zhao C, Alshareef H (2018) Rechargeable aqueous zinc-ion battery based on porous framework zinc pyrovanadate intercalation cathode. *Adv Mater* 30:1705580
32. Zhang N, Cheng F, Liu Y, Zhao Q, Lei K, Chen C, Liu X, Chen J (2016) Cation-deficient spinel $ZnMn_2O_4$ cathode in $Zn(CF_3SO_3)_2$ electrolyte for rechargeable aqueous Zn-Ion battery. *J Am Chem Soc* 138:12894–12901
33. Wang J, Wang J, Liu H, Wei C, Kang F (2019) Zinc ion stabilized MnO_2 nanospheres for high capacity and long lifespan aqueous zinc-ion batteries. *J Mater Chem A* 7:13727

Publisher's note Springer Nature remains neutral with regard to jurisdictional claims in published maps and institutional affiliations.